Inorg. Chem. **2008**, *47*, 10692−10699

Self-Assembly of Triple Helical and *meso*-Helical Cylindrical Arrays Tunable by Bis-Tripodal Coordination Converters

Ji-Jun Jiang,[†] Sheng-Run Zheng,[†] Yu Liu,[†] Mei Pan,[†] Wei Wang,[‡] and Cheng-Yong Su*,[†]

MOE Laboratory of Bioinorganic and Synthetic Chemistry, State Key Laboratory of Optoelectronic Materials and Technologies, School of Chemistry and Chemical Engineering, Sun Yat-Sen University, Guangzhou 510275, China, and State Key Laboratory of Applied Organic Chemistry, Lanzhou University, Lanzhou 730000, China

Received August 9, 2008

The synergistic interplay of coordination and hydrogen-bonding interactions leads to assembly of isomorphous compounds of the general formula $[Ln(ntb)_2](ClO_4)_3 \cdot (BDA4BPy)_3 \cdot 2MeCN\}_\infty$ (Ln = La, Sm and Pr, ntb = tris(2-benzimidazoylmethyl)amine, and BDA4BPy = N^1,N^4-bis(pyridin-4-ylmethylene)-benzene-1,4-diamine), of which polymorphic crystals can be isolated in a different solvent system. In acetonitrile (MeCN) solution, the compounds crystallize as a red color (Ln = La, **meso-1**, Ln = Pr, **meso-2**), while in an acetonitrile−benzonitrile (MeCN−PhCN) mixture, yellow crystals are obtained (Ln = Pr, **helical-2**). The single-crystal X-ray diffraction analyses of these crystals reveal that the structures display similar cylindrical arrays containing polycompartmental cavities for guest inclusion. Occurrence of polymorphism is due to formation of helical and *meso*-helical arrays, giving rise to a way to tune the helicity through the solvent effects on the helix propensity of the bis-tripodal coordination converters.

Introduction

Engineering of supramolecular arrays is currently one of the most important research areas that has implications for the rational design of functional materials.[1] Self-assembly processes that lead to helical motifs are ubiquitous in nature, for example, protein α-helices and the DNA double helix, which have inspired great interest in mimetic synthesis of artificial helical structures aiming at possible applications in material sciences, stereoselective catalysis, and chemical sensing.[2] Two main assembly strategies have emerged depending on the use of coordinative bonds[3] and supramolecular interactions such as hydrogen bonds.[4] A variety of single-, double-, and triple-stranded helical structures have been constructed, showing distinct structural features in either discrete helicates[5] or infinite helices.[6] Another closely related helical entity is the cylindrical array which usually displays helical screw sense.[7]

A key challenge in the assembly of helical structures is to control the helix propensity of subunits which might result in either chiral amplification or helix reversal.[8] In contrast

* To whom correspondence should be addressed. E-mail: cesscy@mail.sysu.edu.cn.
† Sun Yat-Sen University.
‡ Lanzhou University.

(1) (a) Desiraju, G. R. *Angew. Chem., Int. Ed.* **2007**, *46*, 8342. (b) Brammer, L. *Chem. Soc. Rev.* **2004**, *33*, 476. (c) Hagrman, P. J.; Hagrman, D.; Zubieta, J. *Angew. Chem., Int. Ed.* **1999**, *38*, 2638. (d) Dalgarno, S. J.; Thallapally, P. K.; Barbour, L. J.; Atwood, J. L. *Chem. Soc. Rev.* **2007**, *36*, 236. (e) Kitagawa, S.; Kitaura, R.; Noro, S.-i. *Angew. Chem., Int. Ed.* **2004**, *43*, 2334.
(2) (a) Hill, D. J.; Mio, M. J.; Prince, R. B.; Hughes, T. S.; Moore, J. S. *Chem. Rev.* **2001**, *101*, 3893. (b) Greig, L. M.; Philp, D. *Chem. Soc. Rev.* **2001**, *30*, 287. (c) Hannon, M. J. *Chem. Soc. Rev.* **2007**, *36*, 280. (d) Okamoto, Y.; Nakano, T. *Chem. Rev.* **1994**, *94*, 349. (e) Reggelin, M.; Doerr, S.; Klussmann, M.; Schultz, M.; Holbach, M. *Proc. Natl. Acad. Sci. U.S.A.* **2004**, *101*, 5461.
(3) (a) Tanaka, K.; Yamada, Y.; Shionoya, M. *J. Am. Chem. Soc.* **2002**, *124*, 8802. (b) Jung, O.-S.; Kim, Y. J.; Lee, Y.-A.; Park, J. K.; Chae, H. K. *J. Am. Chem. Soc.* **2000**, *122*, 9921. (c) Biradha, K.; Seward, C.; Zaworotko, M. J. *Angew. Chem., Int. Ed.* **1999**, *38*, 492. (d) Kaes, C.; Hosseini, M. W.; Rickard, C. E. F.; Skelton, B. W.; White, A. H. *Angew. Chem., Int. Ed.* **1998**, *37*, 920. (e) Mamula, O.; von Zelewsky, A.; Bark, T.; Bernardinelli, G. *Angew. Chem., Int. Ed.* **1999**, *38*, 2945. (f) Cui, Y.; Ngo, H. L.; Lin, W. *Chem. Commun.* **2003**, 1388.
(4) (a) Davis, J. M.; Tsoub, L. K.; Hamilton, A. D. *Chem. Soc. Rev.* **2007**, *36*, 326. (b) Berl, V.; Krische, M. J.; Huc, I.; Lehn, J.-M.; Schmutz, M. *Chem. Eur. J.* **2000**, *6*, 1938. (c) Berl, V.; Huc, I.; Khoury, R. G.; Krische, M. J.; Lehn, J.-M. *Nature* **2000**, *407*, 720. (d) Hirschberg, J. H. K. K.; Brunsveld, L.; Ramzi, A.; Vekemans, J. A. J. M.; Sijbesma, R. P.; Meijer, E. W. *Nature* **2000**, *407*, 167.
(5) (a) Albrecht, M. *Chem. Rev.* **2001**, *101*, 3457. (b) Piguet, C.; Bernardinelli, G.; Hopfgartner, G. *Chem. Rev.* **1997**, *97*, 2005. (c) Dalla-Favera, N.; Hamacek, J.; Borkovec, M.; Jeannerat, D.; Gumy, F.; Bünzli, J.-C. G.; Ercolani, G.; Piguet, C. *Chem. Eur. J.* **2008**, *14*, 2994.
(6) (a) Han, L.; Hong, M. C. *Inorg. Chem. Commun.* **2005**, *8*, 406. (b) Berl, V.; Huc, I.; Khoury, R. G.; Lehn, J.-M. *Chem. Eur. J.* **2001**, *7*, 2798. (c) Berl, V.; Huc, I.; Khoury, R. G.; Lehn, J.-M. *Chem. Eur. J.* **2001**, *7*, 2810.

10.1021/ic801516b CCC: $40.75
Published on Web 10/16/2008

to the well-studied helical system, the *meso*-helical (sometimes called amphiverse-helical)[9] structures which are characteristic of internal helix reversal remain largely unexplored. The biological examples of *meso*-helices may be found in cycloamylose, tendrils in climbing plants, and B/Z-DNA structures.[10] Moreover, it is known that helical reversion has played an essential role in bacteria swimming which switches its direction of movement by changing the flagellar filament between left- and right-handed helical forms caused by reversal of motor rotation.[11]

Formation of chiral and *meso*-helicates has been well understood, which is controlled either by the length of the alkyl spacer between two bidentate chelating units of the bridging ligand or by a host−guest solvation mechanism.[5,12] Assembly of separately infinite helical or *meso*-helical structures has also been accomplished in coordination and hydrogen-bonding polymers,[13] which may be due to ligand conformational flexibility, supramolecular interactions, or solvent effects. These influencing factors have also been found to be able to tune helical interconversion between right and left handedness.[14] Nevertheless, tuning of a structure between the helical and the *meso*-helical forms has rarely been observed.

We previously reported self-assembly of hydrogen-bonded networks with encapsulated lanthanide(III) coordination units $[Ln(ntb)_2]^{3+}$ [ntb = tris(2-benzimidazoylmethyl)amine] as the building blocks and bipy or bpen (bipy = 4,4′-bipyridyl, bpen = *trans*-1,2-bis(4-pyridyl)ethylene) as spacers, focusing on the stereochemical control by the choice of different spacers.[15] Herein we describe the assembly of triple helical and *meso*-helical cylindrical arrays with the $[Ln(ntb)_2]^{3+}$ subunits acting as the helix converters as shown in Scheme 1 (explained later in the discussion).

Results and Discussion

Syntheses and Crystal Structures. Reaction of the tripodal ligand ntb with $Ln(ClO_4)_3$ (Ln = La, Sm, and Pr) in the presence of the long spacer N^1,N^4-bis(pyridin-4-ylmethylene)-benzene-1,4-diamine (BDA4BPy) readily afforded a series of complexes of the general formula $\{[Ln(ntb)_2](ClO_4)_3 \cdot (BDA4BPy)_3 \cdot 2MeCN\}_\infty$, of which three have been structurally characterized (See Experimental Section). It was found that, in acetonitrile (MeCN) solution, the complexes crystallized as a red color (Ln = La, ***meso*-1**, Ln = Pr, ***meso*-2**), while in an acetonitrile−benzonitrile (MeCN−PhCN) mixture, yellow crystals were obtained (Ln = Pr, ***helical*-2**). The elemental analysis results confirmed the same composition for these complexes, and the single-crystal X-ray diffraction established a similar hydrogen-bonded cylindrical structure as shown in Figure 1. Nevertheless, detailed structural analysis revealed the difference in the propeller conformation of the $[Ln(ntb)_2]^{3+}$ units and screw sense of the BDA4BPy spacers between the red and yellow crystals, leading to formation of distinct helical structures.

In each complex, two ntb ligands display tripod-like tetradentate coordination mode with the central Pr^{3+} (or La^{3+}) ion surrounded by six benzimidazole (Bim) arms, giving rise to a rather similar cationic unit $[Ln(ntb)_2]^{3+}$ as shown in Figure 1a,b. Eight tertiary amine N atoms coordinate with the Ln^{3+} ion to form a slightly distorted cubic environment as observed previously.[15] The Ln−N bond distances show no remarkable features and closely resemble each other (Table 2). Besides four coordinating N donors, each ntb ligand possesses three NH groups which are good hydrogen bond donors. Therefore, the $[Ln(ntb)_2]^{3+}$ unit can provide two sets of N−H···X hydrogen bonds dispositions in opposite directions. Self-assembly of the $[Ln(ntb)_2]^{3+}$ units with the rod-like BDA4BPy spacers results in formation of six N−H···N hydrogen bonds as expected (Figure 1c and Table 3), thus affording a hydrogen-bonded ensemble which features in triple helical multicellular array containing cylindrical internal cavities (Figure 2).

Recognizing the striking difference in helicity of the cylindrical arrays was triggered by observation of distinguishable crystal colors (Figure 3), although all complexes have the same composition. The red complexes ***meso*-1** and **2** crystallize in *R*-3c space groups to make two isomorphous structures, while the yellow complex ***helical*-2** crystallizes in a *R*32 space group, representing a polymorphous structure with complex ***meso*-2**. In addition to the color difference, the polymorphous structures ***meso*-2** and ***helical*-2** show

(7) (a) Baxter, P. N. W.; Lehn, J.-M.; Kneisel, B. O.; Baum, G.; Fenske, D. *Chem. Eur. J.* **1999**, *5*, 102. (b) Baxter, P. N. W.; Lehn, J.-M.; Baum, G.; Fenske, D. *Chem. Eur. J.* **1999**, *5*, 113. (c) Uerpmann, C.; Malina, J.; Pascu, M.; Clarkson, G. J.; Moreno, V.; Rodger, A.; Grandas, A.; Hannon, M. J. *Chem. Eur. J.* **2005**, *11*, 1750. (d) Son, S. U.; Park, K. H.; Kim, B. Y.; Chung, Y. K. *Cryst. Growth & Des.* **2003**, *3*, 507.

(8) (a) Dolain, C.; Léger, J.-M.; Delsuc, N.; Gornitzka, H.; Huc, I. *Prod. Natl. Acad. Sci. U.S.A.* **2005**, *102*, 16146. (b) Maurizot, V.; Dolain, C.; Leydet, Y.; Léger, J.-M.; Guionneau, P.; Huc, I. *J. Am. Chem. Soc.* **2004**, *126*, 10049. (c) Sakurai, S.-i.; Ohsawa, S.; Nagai, K.; Okoshi, K.; Kumaki, J.; Yashima, E. *Angew. Chem., Int. Ed.* **2007**, *46*, 7605. (d) Okoshi, K.; Sakurai, S.-i.; Ohsawa, S.; Kumaki, J.; Yashima, E. *Angew. Chem., Int. Ed.* **2006**, *45*, 8173.

(9) (a) Brewster, J. H. *Top. Curr. Chem.* **1974**, *47*, 29. (b) Floquet, S.; Ouali, N.; Bocquet, B.; Bernardinelli, G.; Imbert, D.; Bünzli, J.-C. G.; Hopfgartner, G.; Piguet, C. *Chem. Eur. J.* **2003**, *9*, 1062.

(10) (a) Luger, P. *Angew. Chem., Int. Ed.* **1998**, *37*, 3353. (b) Goriely, A.; Tabor, M. *Phys. Rev. Lett.* **1998**, *80*, 1546. (c) Ha, S. C.; Lowenhaupt, K.; Rich, A.; Kim, Y.-G.; Kim, K. K. *Nature* **2005**, *437*, 1183.

(11) (a) Samatey, F. A.; Imada, K.; Nagashima, S.; Vonderviszt, F.; Kumasaka, T.; Yamamoto, M.; Namba, K. *Nature* **2001**, *410*, 331. (b) Yonekura, K.; Maki-Yonekura, S.; Namba, K. *Nature* **2003**, *424*, 643. (c) Mühling, M.; Harris, N.; Belay, A.; Whitton, B. A. *J. Phycol.* **2003**, *39*, 360. (d) Schmitt, R. *Biophys. J.* **2003**, *85*, 843.

(12) (a) Xu, J.; Parac, T. N.; Raymond, K. N. *Angew. Chem., Int. Ed.* **1999**, *38*, 2878. (b) Albrecht, M. *Chem. Eur. J.* **2000**, *6*, 3485. (c) Constable, E. C.; Neuburger, M.; Whall, L. A.; Zehnder, M. *New J. Chem.* **1998**, 219.

(13) (a) Cai, Y.-P.; Zhang, H.-X.; Xu, A.-W.; Su, C.-Y.; Chen, C.-L.; Liu, H.-Q.; Zhang, L.; Kang, B.-S. *J. Chem. Soc., Dalton Trans.* **2001**, 2429. (b) Plasseraud, L.; Maid, H.; Hampel, F.; Saalfrank, R. W. *Chem. Eur. J.* **2001**, *7*, 4007. (c) Blay, G.; Fernández, I.; Pedro, J. R.; Ruiz-García, R.; Muñoz, M. C.; Cano, J.; Carrasco, R. *Eur. J. Org. Chem.* **2003**, 1627. (d) McMorran, D. A. *Inorg. Chem.* **2008**, *47*, 592. (e) Luan, X.-J.; Wang, Y.-Y.; Li, D.-S.; Liu, P.; Hu, H.-M.; Shi, Q.-Z.; Peng, S.-M. *Angew. Chem., Int. Ed.* **2005**, *44*, 3864.

(14) (a) Engelkamp, H.; Middelbeek, S.; Nolte, R. J. M. *Science* **1999**, *284*, 785. (b) Yashima, E.; Maeda, K.; Okamoto, Y. *Nature* **1999**, *399*, 449. (c) Barboiu, M.; Vaughan, G.; Kyritsakas, N.; Lehn, J.-M. *Chem. Eur. J.* **2003**, *9*, 763.

(15) (a) Su, C.-Y.; Kang, B.-S.; Liu, H.-Q.; Wang, Q.-G.; Mak, T. C. W. *Chem. Commun.* **1998**, 1551. (b) Su, C.-Y.; Kang, B.-S.; Yang, Q.-C.; Mak, T. C. W. *J. Chem. Soc., Dalton Trans.* **2000**, 1857.

Scheme 1. Schematic Procedure for Self-Assembly of the Helical and *meso*-Helical Cylindrical Arrays[a]

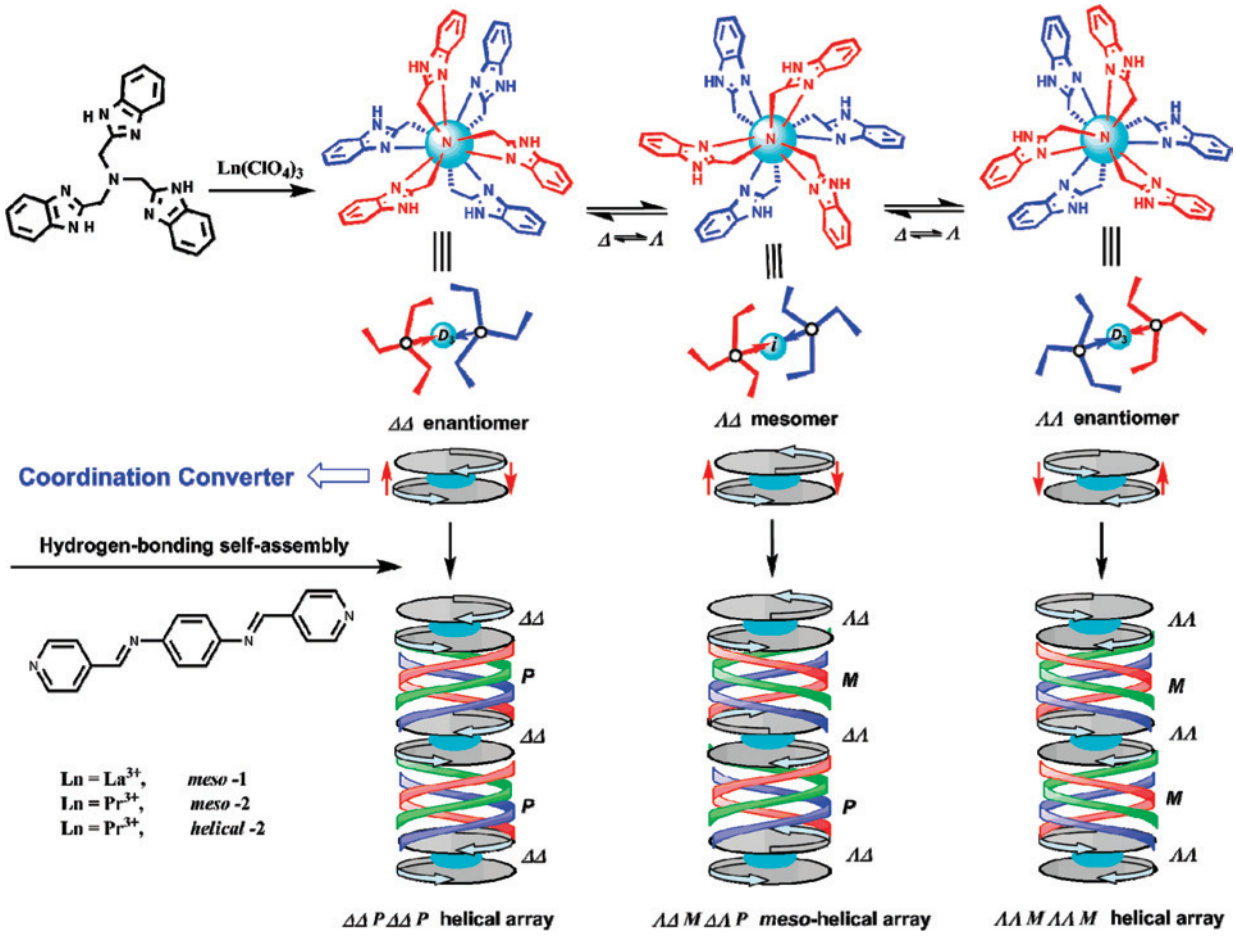

[a] In representatives of enantiomer and mesomer, straight arrows indicate the view direction and warped arrows indicate clockwise or anticlockwise propeller fashion.

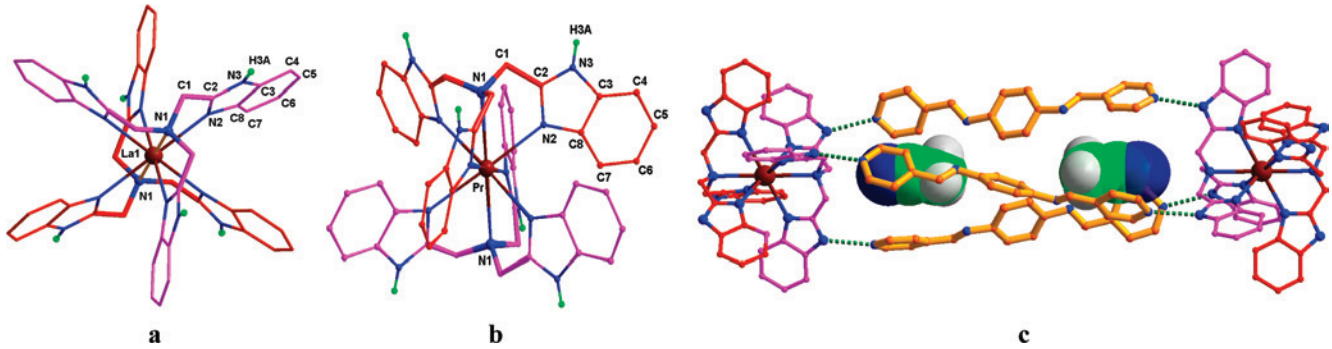

Figure 1. The cationic $[Ln(ntb)_2]^{3+}$ units in complexes: (a) ***meso*-1** and (b) ***helical*-2**, showing atomic labeling and propeller conformation of two ntb ligands differentiated by colors. (c) Hydrogen-bonded triple helical cylindrical motif encapsulating acetonitrile guest molecules.

distinguishable patterns in their powder X-ray diffraction (XRD) (Figure S1 and S2, Supporting Information). Moreover, a significant difference in their thermal stability measurements was observed (Figure 4). Thermogravimetric analysis (TGA) suggested that the guest MeCN molecules in both structures escaped gradually upon increasing of the temperature; however, they were lost comparatively faster in the ***helical*-2** than in the ***meso*-2**. The succeeding decomposition steps of the cylindrical arrays are also different: a sharp weight loss occurred in ***helical*-2** immediately, while ***meso*-2** started with a slow weight loss.

The above-mentioned physical properties normally correlate with the crystal habit which is inherent in the structural nature; therefore, careful crystal structure examination is necessary to understand the structure−property relationship. It is well-known that the tripodal ligand can take the C_3 symmetry to impose intrinsic chirality when the three pendants adopt *syn,syn,syn*-conformation to display propeller-like arrangement.[16] For the ML_2 type bis-tripodal complexes, two tripodal ligands usually exhibit the same handed propeller fashions when viewed from the apical central atom of the ligand down to the metal ion,[15,17] thus endowing

Table 1. Crystal Data and Structure Refinement Parameters for Complexes

	meso-1	meso-2	helical-2
empirical formula	$C_{106}H_{90}Cl_3LaN_{28}O_{12}$	$C_{106}H_{90}Cl_3PrN_{28}O_{12}$	$C_{106}H_{90}Cl_3PrN_{28}O_{12}$
fw	2193.32	2195.32	2195.32
crystal syst	trigonal	trigonal	trigonal
space group	*R*-3c	*R*-3c	*R*32
a (Å)	17.987(5)	17.8881(5)	17.8687(4)
c (Å)	53.73(2)	53.590(2)	26.7725(10)
V (Å^3)	15054(9)	9354(3)	7795.9(8)
Z	6	6	3
D_{calc} (g cm^{-3})	1.452	1.473	1.477
μ (mm^{-1})	0.584	0.652	0.654
T (K)	293(2)	150(2)	150(2)
R_1	0.0628	0.0754	0.0699
wR_2	0.1732	0.1919	0.1753

Table 2. Selected Bond Lengths (Å) and Bond Angles (°) for **meso-1**, **meso-2**, and **helical-2**[a]

meso-1			
La(1)−N(2)	2.643(5)	La(1)−N(1)	2.827(6)
N(2)#1−La(1)−N(2)	100.37(12)	N(2)#1−La(1)−N(2)	79.63(12)
N(2)−La(1)−N(1)	62.49(9)	N(2)#2−La(1)−N(1)	117.51(9)
N(1)#2−La(1)−N(1)	180.0	N(2)#2−La(1)−N(2)	180.00(16)
meso-2			
Pr(1)−N(1)	2.610(5)	Pr(1)−N(3)	2.802(7)
N(1)−Pr(1)−N(1)#1	101.04(13)	N(1)#2−Pr(1)−N(1)#3	78.96(13)
N(1)#1−Pr(1)−N(3)	63.03(11)	N(1)#3−Pr(1)−N(3)	116.97(11)
N(1)−Pr(1)−N(1)#3	180.00(19)	N(3)−Pr(1)−N(3)#3	180.00
helical-2			
Pr−N(1)	2.803(4)	Pr−N(2)	2.582(3)
N(2)#2−Pr−N(2)	100.86(9)	N(2)#c−Pr−N(2)	76.42(14)
N(2)−Pr−N(1)	62.89(7)	N(2)#1−Pr−N(1)	117.11(7)
N(2)#1−Pr−N(2)#2	176.49(16)	N(1)−Pr−N(1)#4	180.000(1)

[a] Symmetry codes for **meso-1**: #1, $x - y + 1, x + 1, -z$; #2, $-x, -y + 2, -z$; #3, $-x + y - 1, -x + 1, z$. **meso-2**: #1, $-x + y + 1, -x + 2, z$; #2, $-y + 2, x - y + 1, z$; #3, $-x + 2, -y + 2, -z$. **helical-2**: #1, $-x, -x + y, -z + 5/2$; #2, $-y + 1, x - y + 2, z$; #3, x −y + 1, −y + 2, $-z + 5/2$; #4, $y - 1, x + 1, -z + 5/2$.

normalized D_3 symmetry to the chiral coordination motif. On the contrary, once two tripodal ligands display both clockwise (Δ) and anticlockwise (Λ) propeller fashions, inversion symmetry can be imposed on the metal center (refer to Scheme 1), thus forming an achiral mesomer. Such ML_2 tripodal mesomer has rarely been observed, which obviously provides a coordination converter being able to tune the chirality. As seen from Figure 1a,b, the $[Ln(ntb)_2]^{3+}$ unit in complex ***meso*-1** (or ***meso*-2**) comprises two reversely handed ntb ligands (denoted as ΛΔ-mesomer), while that in ***helical*-2** consists of two same handed ntb ligands (denoted as ΛΛ/ΔΔ-enantiomer).

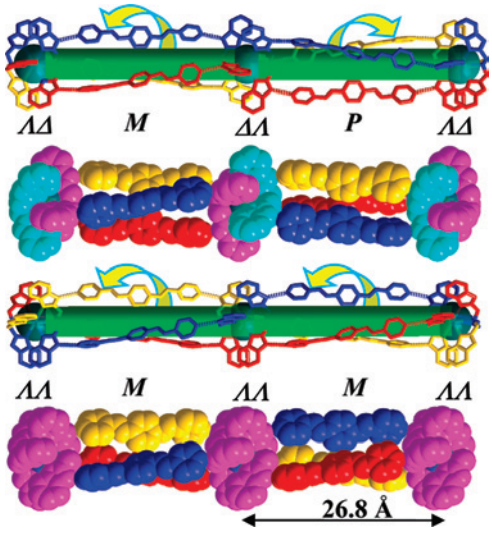

Figure 2. The *meso*-helical cylindrical arrays in ***meso*-1**/***meso*-2** (upper) and helical cylindrical array in ***helical*-2** (lower). The triply screw arrangement of BDA4BPy spacers is indicated by arrows, and compartmental cavities formed inside cylinders are represented by green rods.

The structural analysis also revealed that the BDA4BPy spacers wrap around a C_3-axis showing a screw sense. Therefore, the triple-stranded capsular motif $[Ln(ntb)_2]$-$(BDA4BPy)_3$-$[Ln(ntb)_2]$ (Figure 1c) can be described as either a *P* (right-handed) or an *M* (left-handed) helical cylinder depending on the screw sense of the three BDA4BPy spacers (refer to Scheme 1). A noticeable finding is that the three same screw-handed BDA4BPy spacers join two same propeller-handed ntb ligands at the two ends, indicating a chiral transfer through the N−H···N hydrogen-bonding recognition. However, because the $[Ln(ntb)_2]^{3+}$ units can be either enantiomers or mesomers, the overall helicity of the cylindrical array is consequently controlled by the coordination converters. For example, the ***helical*-2** can display either ΔΔ*P*ΔΔ*P* or ΛΛ*M*ΛΛ*M* helical arrays, while the ***meso*-2** may exhibit either ΛΔ*M*ΔΛ*P* or ΔΛ*M*ΛΔ*P* *meso*-helical arrays.

The different helical arrays cause significantly different crystal packing modes as shown in Figure 3 and Figure S3, Supporting Information. Although both helical and *meso*-helical arrays are aligned in parallel along the *c*-axis in the crystal lattice, the orientations of the BDA4BPy spacers are clearly different. In ***helical*-2** there is only one type of conformation of spacers which show the same handedness, while in ***meso*-2** there are two types of inverted conformations of spacers with *P* and *M* handedness coexisting. The uniform arrangement of the BDA4BPy spacers in ***helical*-2** gives rise to the strictly ordered crystal packing, which causes distinct components distribution and vacant space in the crystal lattice compared with that in ***meso*-2**. For instance, more permeable one-dimensional channels are formed in ***helical*-2** in the *c* direction. This may be the reason why the guest molecules are easily removed at lower temperature, but the framework collapses abruptly for ***helical*-2** in contrast to that for ***meso*-2**. Moreover, the different crystal packing may result in light transmission difference in the crystal lattice, which may account for the different color of ***meso*-2** and ***helical*-2**, indicating that the specific conformation of the spacers may correlate with special electronic structure. Such difference in physicochemical property is often observed between the polymorphous crystals; nevertheless, the intrinsic physical mechanism remains unknown and waits for further investigation.

(16) (a) Moberg, C. *Angew. Chem., Int. Ed.* **1998**, *37*, 248. (b) Katsuki, I.; Motoda, Y.; Sunatsuki, Y.; Matsumoto, N.; Nakashima, T.; Kojima, M. *J. Am. Chem. Soc.* **2002**, *124*, 629. (c) Zhang, X.-L.; Guo, C.-P.; Yang, Q.-Y.; Wang, W.; Liu, W.-S.; Kang, B.-S.; Su, C.-Y. *Chem. Commun.* **2007**, 4242.

(17) (a) Su, C.-Y.; Kang, B.-S.; Liu, H.-Q.; Wang, Q.-G.; Chen, Z.-N.; Lu, Z.-L.; Tong, Y.-X.; Mak, T. C. W. *Inorg. Chem.* **1999**, *38*, 1374. (b) Cai, Y.-P.; Su, X.-Y.; Chen, C.-L.; Li, Y.-M.; Kang, B.-S.; Chan, A. S. C.; Kaim, W. *Inog. Chem.* **2003**, *42*, 163.

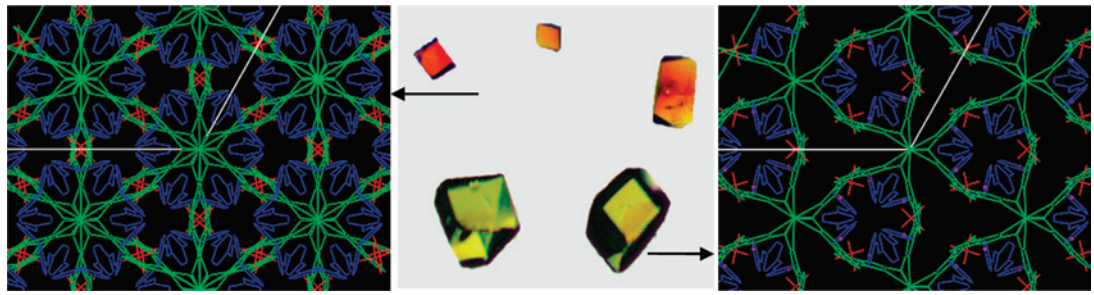

Figure 3. Crystals picture showing different colors for ***meso*-1**, ***meso*-2** (red), and ***helical*-2** (yellow), and their respective crystal packing in the *ab* plane.

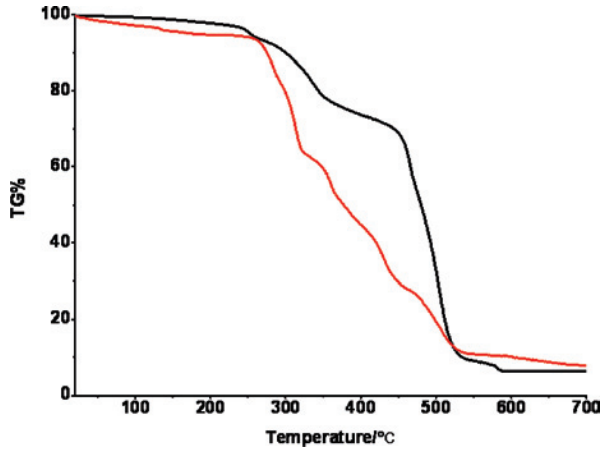

Figure 4. TG analyses of complexes ***meso*-2** (black) and ***helical*-2** (red).

Solution Structures and Assembly Mechanism. To explore the self-assembly procedure of the helical and *meso*-helical arrays, solution structures have been studied by means of the ESI-MS and ^{1}H NMR methods for the Sm^{3+} complex because the Sm^{3+} ion has weak paramagnetism with negligible influence on the NMR line broadening and appropriate kinetic inertness to detect ligand exchange process.[18] As shown in Figure 5, a 1:2 mixture of $Sm(ClO_4)_3 \cdot 6H_2O$ and ntb ligand in CD_3CN (10^{-3} M) at 293 K gives one set of proton signals corresponding to "free" ligand; however, the aromatic signals from the Bim rings shift upfield while the methylene signal remains almost unchanged. This consists with the formation of $[Sm(ntb)_2]^{3+}$ species where six Bim rings from two ligands shield each other due to interdigitated arrangement (Figure 1). Another evidence for exclusive formation of $[Sm(ntb)_2]^{3+}$ species in solution comes from ESI-MS measurements (Figure 6). The only major peak (*m*/*z* 533.5) is assignable to $[Sm(ntb)_2(ClO_4)]^{2+}$ which is verified by the exact match of the isotopic distribution with the theoretical simulation.[18,19] An interesting finding is that the water signal shifts remarkably downfield to overlap with the methylene signal, indicative of N−H···O hydrogen-bonding interaction between the ligand NH group and water molecules. Careful examination of NMR spectrum confirms that the methylene signal is sharp and enantiotopic. These results imply that the three Bim arms of the two ligands are equivalent and rotatable about the $N-C_{methylene}$ bonds, leading to a pseudo-D_{3h} symmetry as a results of fast $\Delta \rightleftharpoons \Lambda$ intramolecular interconversion on the NMR time scale at 293 K.[18] Because each $[Sm(ntb)_2]^{3+}$ unit contains two ntb ligands, the dynamic interconversion process should be averaged from three final states, namely, $\Delta\Delta$, $\Lambda\Lambda$ enantiomers and $\Lambda\Delta$ mesomer (see Scheme 1).

When the BDA4BPy spacers were added in an M:L:spacer molar ratio of 1:2:3 at 293 K, the NMR spectrum displayed well assignable proton sets containing both the ntb ligand and the BDA4BPy spacer. The signals from the Bim rings are comparable with those of "free" $[Sm(ntb)_2]^{3+}$, but the methylene and NH signals are significantly broadened (assignment verified by D_2O exchange). The spectra of the M:L:spacer molar ratios of 1:2:2 and 1:2:4 show a similar feature with slightly different broadening of the methylene singals, indicating that different helical precursors associated with the N−H···N hydrogen-bonding $[Ln(ntb)_2]^{3+}$-spacers are formed but still dynamically averaged at room temperature. Broadening of the methylene signals suggests that the fast $\Delta \rightleftharpoons \Lambda$ interconversion has been slowed down due to formation of the N−H···N hydrogen bonds. Therefore, the variable temperature NMR measurements were carried out for the 1:2:3 system (293−258 K). It was found that the methylene signal became diastereotopic when the temperature decreased. These findings verify that the rotation of the Bim rings are hindered after formation of the N−H···N hydrogen bonds. The propeller conformation of the ligand will be blocked to C_3-symmetry when the $[Sm(ntb)_2]^{3+}$ converters are prohibited from fast $\Delta \rightleftharpoons \Lambda$ interconversion. Coalescence of the two methylene signals occurs at about 295 K, which results in an estimated energy barrier ΔG of 56 kJ mol^{-1} for the dynamic helical interconversion.[18,19] This interconversion energy barrier may be mainly contributed from the N−H···N hydrogen-bonding interactions as well as the ligand exchange.

On the basis of the above solution structural results, a possible self-assembly procedure is proposed as depicted in Scheme 1. At room temperature, the thermodynamic solution species $[Ln(ntb)_2]^{3+}$ coexisting as $\Delta\Delta$, $\Lambda\Lambda$ enantiomers and $\Lambda\Delta$ mesomers establish an equilibrium with $\Delta \rightleftharpoons \Lambda$ interconversions occurring. Upon self-assembly with BDA4BPy spacers through N−H···N hydrogen-bonding, the kinetic control of the solution to crystal interfacing phase transfer

(18) (a) Renaud, F.; Piguet, C.; Bernardinelli, G.; Biinzli, J.-C. G.; Hopfgartner, G. *Chem. Eur. J.* **1997**, *3*, 1646. (b) Renaud, F.; Piguet, C.; Bernardinelli, G.; Biinzli, J.-C. G.; Hopfgartner, G. *J. Am. Chem. Soc.* **1999**, *121*, 9326.

(19) (a) Chen, C.-L.; Tan, H.-Y.; Zhang, Q.; Yao, J.-H.; Su, C.-Y. *Inorg. Chem.* **2005**, *44*, 8510. (b) Su, C.-Y.; Cai, Y.-P.; Chen, C.-L.; Smith, M. D.; Kaim, W.; zur Loye, H.-C. *J. Am. Chem. Soc.* **2003**, *125*, 8595.

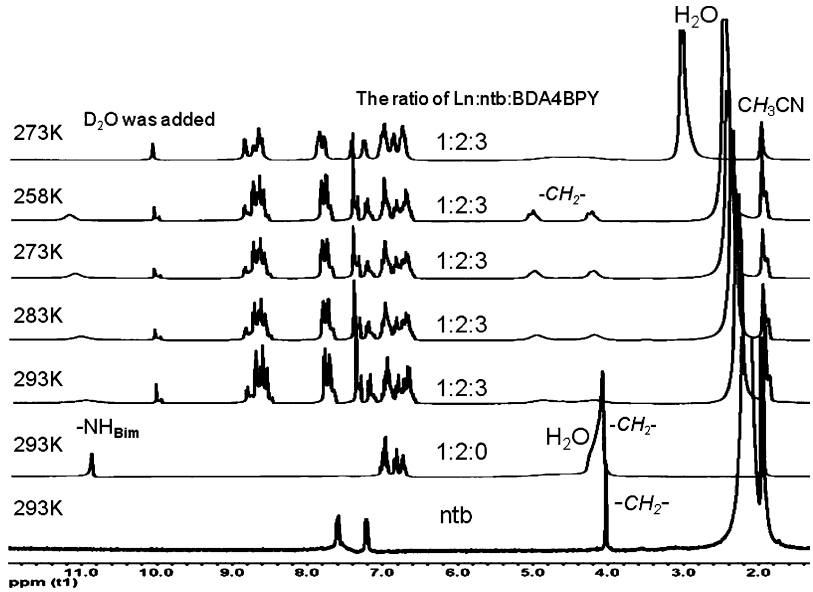

Figure 5. Titration of the ligand ntb with $Sm(ClO_4)_3 \cdot 6H_2O$ and BDA4BPy in CD_3CN, and VT ^1H NMR spectra in an M:L:spacer ratio of 1:2:3.

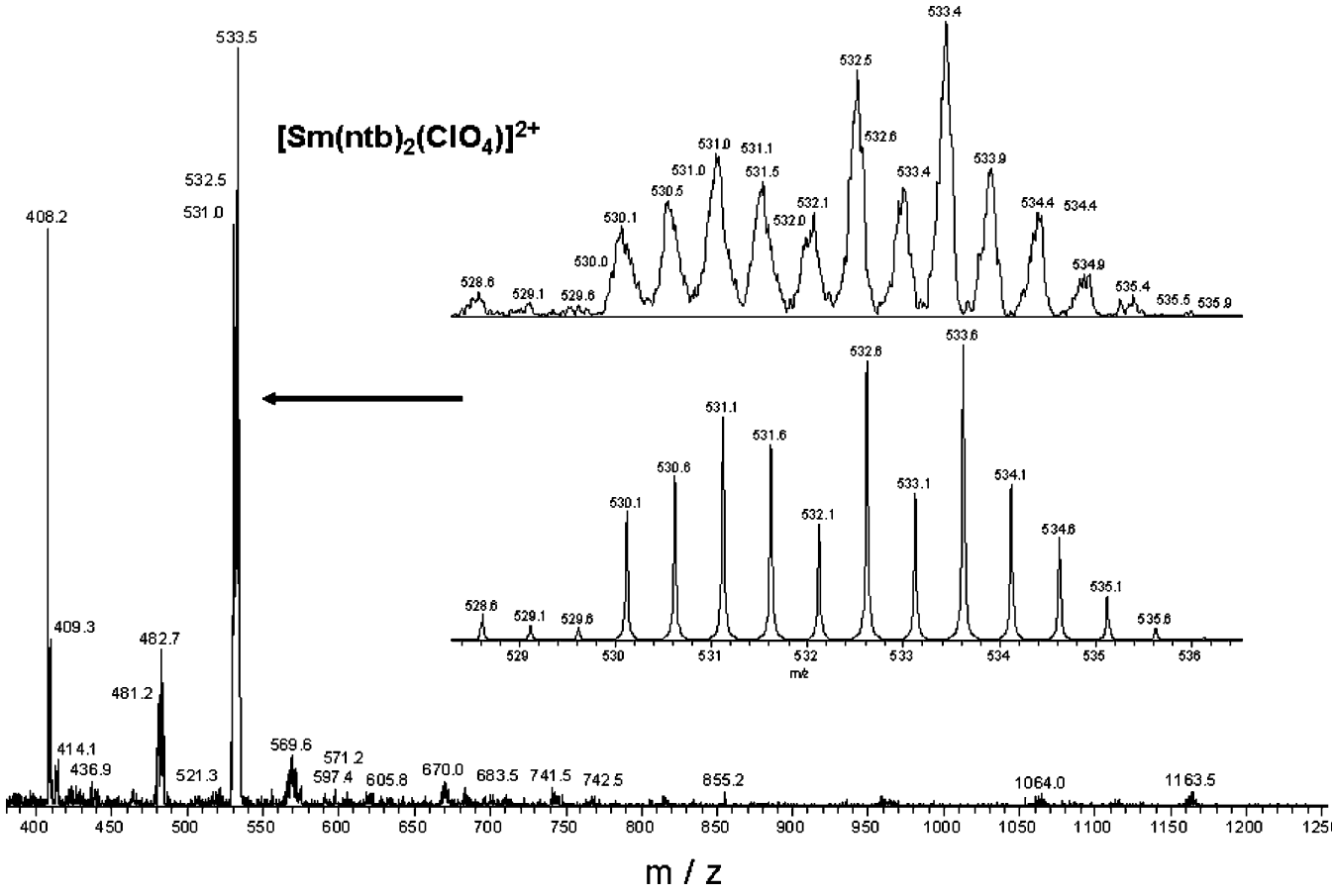

Figure 6. ESI-MS spectrum of a solution of $Sm(ClO_4)_3 \cdot 6H_2O$ and ligand ntb with 1:2 ratio in MeCN (10^{-3} M). Isotopic distribution of the double-charged $[Sm(ntb)_2(ClO_4)]^{2+}$ motif with the theoretical simulation shown in the inset.

takes place to crystallize. Since the helical precursors associated with the hydrogen-bonding $[Ln(ntb)_2]^{3+}$-spacers are interconvertible with relatively low energy barrier ΔG of 56 kJ mol^{-1}, the subtle influence on the crystallization condition may be able to direct the self-assembly procedure when the conformation of the tripodal ligand is blocked. Because three helical BDA4BPy spacers prefer to recognize two same handed tripodal ligands, the helical propagation is subject to the selection of ML_2 coordination converters. If enantiomers are assembled, a $\Delta\Delta P\Delta\Delta P$ or $\Lambda\Lambda M\Lambda\Lambda M$ helical array will be formed. On the contrary, once the mesomers are selected, an $\Lambda\Delta M\Delta\Lambda P$ or $\Delta\Lambda M\Lambda\Delta P$ *meso*-helical array will result due to alternate helix reversal. Therefore, the $[Ln(ntb)_2]^{3+}$ units act as bis-tripodal coordina-

Table 3. Hydrogen Bonds Geometry in Complexes **meso-1**, **meso-2**, and **helical-2**

	D−H, Å	H···A, Å	D···A, Å	∠D−H···A, deg
***meso*-1**	0.88	2.00	2.791(8)	149.2
***meso*-2**	0.86	1.95	2.783(7)	164.4
***helical*-2**	0.88	1.89	2.757(6)	167.9

tion converters to tune the helicity of the cylindrical array, offering a new approach to switch helical structures[8] comparable with the motor rotation mechanism in bacteria.[11]

It is noteworthy that, no matter the self-assembly process started from a chiral ML_2 unit or from an achiral one, the successive selection of the ML_2 units is not arbitrary but consistent with the initial one. This means that the common role of chiral memory and transfer in synergistic assembly is effective in construction of present helical and *meso*-helical arrays. One of the important influencing factors in such uniform self-assembly may be the solvent environment which is proven to be able to facilitate formation of helical structure with preferred handedness.[14] We have tested the following solvent systems for crystallization: (i) MeCN, (ii) MeCN + EtOH, (iii) MeCN + PhCN, (iv) MeCN + EtOH + PhCN, (v) MeCN + THF, and (vi) MeCN+$CHCl_3$. In cases of v and vi, assembly of hydrogen-bonding structure failed probably due to competition of N−H···O and N−H···Cl hydrogen bonds versus N−H···N hydrogen bonds. The solvent system iv gave rise to simultaneous crystallization of both red and yellow crystals, indicative of inefficient chiral preference. Uniform formation of helical structure was achieved in case iii while that of *meso*-helical structure in cases i and ii. A possible reason why the PhCN solvent environment prefers a helical structure to a *meso*-helical one is that the aromatic ring of PhCN can effectively interact with ntb ligands and BDA4BPy spacers via $\pi\cdots\pi$ stacking.[16] This may reduce fast interconversion of ntb conformations and therefore make self-organization and helix propensity control easier.

The host−guest interaction may also play an important role in formation of helical structures.[12a] Since the cylindrical cavity provides a long but narrow host environment, the MeCN molecule was discriminated from other solvent molecules for inclusion because of the perfect complementary match. However, the linear nature of the MeCN guest, although effective as a template to induce formation of helical cylinder, makes little contribution to the helical control. The helix propensity of $[Ln(ntb)_2]^{3+}$ units is obviously more affected by the planar aromatic PhCN solvent than the linear MeCN solvent, although PhCN molecules are not suitable guests for inclusion.

Conclusion

In summary, triple helical and *meso*-helical cylindrical structures have been obtained from synergistic assembly of bis-tripodal complex units and bifunctional spacers on the basis of coordination-binding and hydrogen-bonding interactions. Tuning of the helical arrays is achieved through solvent effects on the helix propensity of bis-tripodal coordination converters. Solution structures have been studied in an effort to understand the self-assembly procedure. The self-organization processes of the cylindrical arrays presented here features in (a) inerrant N−H···N hydrogen-bonding recognition between the linear spacers and the tripodal ligands responsible for assembly of cylindrical cages encapsulating MeCN guests, (b) stereochemical recognition between the screw sense of the spacers and propeller conformation of the ligands leading to local chirality transfer from one end to another, and (c) memorized selection of the ML_2 motifs in self-assembly process keeping helical propagation based on the enantiomers or helix reversal based on the mesomers. Finally, polymorphism of ***meso*-2** and ***helical*-2** complexes leads to not only a chiral difference, but also physicochemical differences in color and thermal behaviors.

Experimental Section

Syntheses and Characterization: $\{[La(ntb)_2](ClO_4)_3\cdot(BDA\text{-}4BPy)_3\cdot 2MeCN\}_\infty$, meso-1. A solution of $La(ClO_4)_3\cdot 6H_2O$ (0.014 g, 0.025mmol) in 2 mL of MeCN was added to a suspension of ligand ntb (0.020 g, 0.05mmol) in 2 mL of acetonitrile (MeCN) with constant stirring. To this mixture BDA4BPy (0.086 g, 0.3 mmol) was slowly added. The resulting mixture was heated for half an hour to produce a clear solution. Slow diffusion of diethyl ether into the mixture over 24 h afforded red block crystals. Yield: 68%. Anal. Calcd for $LaC_{106}H_{90}Cl_3N_{28}O_{12}$: C, 58.05; H, 4.14, N, 17.88. Found: C, 57.37; H, 4.10; N, 17.40%. IR (KBr, cm^{-1}): 3425, 3348, 3187, 3117, 3058, 2981, 2889, 2754, 2463, 1859, 1601, 1558, 1450, 1418, 1347, 1269, 1212, 1093, 1026, 839, 750, 622, 562.

$\{[Pr(ntb)_2](ClO_4)_3\cdot(BDA4BPy)_3\cdot 2MeCN\}_\infty$, *meso*-2. This complex was synthesized in the same way as complex ***meso*-1** by using $Pr(ClO_4)_3\cdot 6H_2O$ (0.014 g, 0.025 mmol) instead of $La(ClO_4)_3\cdot 6H_2O$ (0.014 g, 0.025mmol). Yield: 65%. Anal. Calcd for $PrC_{106}H_{90}Cl_3N_{28}O_{12}$: C, 57.99; H, 4.13; N, 17.86. Found: C, 56.44; H, 4.34, N, 16.15%. IR (KBr, cm^{-1}): 3452, 3354, 3192, 3056, 2988, 2890, 2757, 2464, 1907, 1604, 1468, 1450, 1417, 1320, 1269, 1211, 1092, 1028, 843, 750, 623, 563.

$\{[Pr(ntb)_2](ClO_4)_3\cdot(BDA4BPy)_3\cdot 2MeCN\}_\infty$, *helical*-2. A solution of $Pr(ClO_4)_3\cdot 6H_2O$ (0.014 g, 0.025 mmol) in 1 mL of MeCN was added to a suspension of ligand ntb (0.020 g, 0.05mmol) in 1 mL of acetonitrile (MeCN) with constant stirring. To this mixture BDA4BPy (0.086 g, 0.3 mmol) was slowly added, and then 5 mL of benzonitrile was added. The resulting mixture was heated for half an hour to produce a clear solution. Slow diffusion of diethyl ether into the mixture over 48 h afforded yellow block crystals. Yield 83%. Anal. Calcd for $PrC_{106}H_{90}Cl_3N_{28}O_{12}$: C, 57.99; H, 4.13; N, 17.86. Found: C, 56.76; H, 4.52; N, 17.34%. IR (KBr, cm^{-1}): 3436, 3356, 3189, 3052, 2986, 2889, 2758, 2460, 1914, 1637, 1567, 1450, 1434, 1320, 1270, 1149, 1078, 840, 750, 626, 562.

Physical Methods. IR spectra were measured on a Nicolet/Nexus-670 FT-IR spectrometer with KBr pellets in the range 4000−400 cm^{-1}. The C, H, and N elemental analyses were performed on a Perkin-Elmer 240 elemental analyzer. Thermogravimetric analyses (TGA) were carried out on a Netzsch/TG209F3 instrument under 1 atm pressure at a heating rate of 10 °C min^{-1}. Powder X-ray diffraction (XRD) data were recorded on a Bruker D8 ADVANCE X-ray powder diffractometer (Cu Kα, 1.5418 Å).

Crystal Structure Determination. Single-crystal reflection data were collected on a Bruker Smart 1K CCD diffractometer using Mo−Kα radiation ($\lambda = 0.71073$ Å) using the ω-2θ scan technique for ***meso*-1** and on an Oxford Gemini S Ultra diffractometer with the Enhance X-ray Source of Mo−Kα radiation ($\lambda = 0.71073$ Å) using the ω-φ scan technique for ***meso*-2** and ***helical*-2**. Structural

solution and refinement against F^2 were carried out using the SHELXL programs.[20] The ClO_4^- anion in ***helical*-2** is disordered with four O atoms occupying two sets of positions and refined with a tetrahedral model. The crystal displays racemic twining with the BASF parameter of 0.49. Crystallographic data for the structures reported in this paper have been deposited with the Cambridge Crystallographic Data Centre as supplementary publication no. CCDC 684605−684607. Crystallographic data and other pertinent information for complexes are summarized in Table 1. Selected bond lengths and bond angles are listed in Tables 2 and 3.

(20) Sheldrick, G. M. *SHELX 97, Program for Crystal Structure Solution and Refinement*, Göttingen University, 1997.

Acknowledgment. This work was supported by the NSF for Distinguished Young Scholars of China (Grant 20525310), 973 Program of China (Grant 2007CB815302), the NSF of China (Grants 20673147, 20773167, 20731005), and RFDP of Higher Education.

Supporting Information Available: X-ray crystallographic data (CIF), Powder XRD patterns and crystal packing figures. This material is available free of charge via the Internet at http://pubs.acs.org.

IC801516B